

Antiferromagnetic order in Co-doped Fe_5GeTe_2 probed by resonant magnetic x-ray scattering

Xiang Chen,^{1,2,*} Enrico Schierle,³ Yu He,^{4,2,1} Mayia Vranas,⁵ John William Freeland,⁶ Jessica L. McChesney,⁶ Ramamoorthy Ramesh,^{7,1,2} Robert J. Birgeneau,^{2,1,7} and Alex Franco^{5,†}

¹Materials Science Division, Lawrence Berkeley National Lab, Berkeley, California 94720, USA

²Physics Department, University of California, Berkeley, California 94720, USA

³Helmholtz-Zentrum Berlin für Materialien und Energie, BESSY II, D-12489 Berlin, Germany.

⁴Department of Applied Physics, Yale University, New Haven, Connecticut, 06511, USA

⁵Department of Physics, University of California, San Diego, California 92093, USA

⁶Advanced Photon Source, Argonne National Laboratory, Argonne, Illinois 60439, USA

⁷Department of Materials Science and Engineering,
University of California, Berkeley, California 94720, USA

(Dated: August 1, 2022)

The quasi-two-dimensional van der Waals magnet $\text{Fe}_{5-\delta}\text{GeTe}_2$ has emerged as a promising platform for electronic and spintronic functionalities at room temperature, owing to its large ferromagnetic ordering temperature $T_C \sim 315$ K. Interestingly, by cobalt (Co) substitution of iron in F5GT, *i.e.* $(\text{Fe}_{1-x}\text{Co}_x)_{5-\delta}\text{GeTe}_2$ (Co-F5GT), not only can its magnetic transition temperature be further enhanced, but the magnetic and structural ground states can also be tuned. Specifically, an antiferromagnetic (AFM) order is induced beyond the Co doping level $x \geq 0.4$. Here, we investigate the magnetic properties of a Co-F5GT single crystal at $x = 0.45(1)$, by utilizing the element specific, resonant magnetic x-ray scattering technique. Our study reveals an A-type, Ising-like AFM ground state, with a transition temperature $T_N \sim 340$ K. In addition, our work unveils an important contribution from Co magnetic moments to the magnetic order. The application of the in-plane magnetic fields gradually polarize the spin moments along the field direction, but without inducing incommensurate spin texture(s).

The unique nature of the cleavable, quasi-two-dimensional (quasi-2D) van der Waals (vdW) materials offers rich platforms for exploring both exotic physical phenomena and technological applications [1–9]. A broad variety of intriguing physical phenomena have been reported in recent years by investigating the (atomically thin) vdW bonded compounds. Some exceptional phenomena include unconventional superconductivity in twisted graphene [10], nonlinear Hall effect in few-layer WTe_2 [11, 12], 2D magnetism in monolayer $\text{Cr}_2\text{Ge}_2\text{Te}_6$ [13, 14], CrI_3 [15, 16] and the quantum anomalous Hall effect in insulating tellurides [17, 18]. Among the different materials, the layered vdW, itinerant magnets represent ideal quasi-2D material systems which enable the coupling between the electronic and magnetic degrees of freedom [1, 4–7]. Therefore, vast opportunities arise because of the rich physical properties and the abundant possibilities for functional devices [19, 20].

Very recently, some promising quasi-2D magnetic tellurides [21–33], such as Fe_5GeTe_2 (F5GT) and CrTe_2 , with atomically thin nanoflakes for promising room temperature (RT) spintronics have been reported. The F5GT compound has a ferromagnetic (FM) transition above RT at $T_C \sim 315$ K [30, 31]. Intriguingly, with cobalt (Co) substitution of iron (Fe) in F5GT $(\text{Fe}_{1-x}\text{Co}_x)_{5-\delta}\text{GeTe}_2$, (Co-F5GT), the magnetic transition temperature is further increased up to ~ 360 K, and the magnetic ground state switches from FM to antiferromagnetic (AFM) when the Co doping level reaches $x \geq 0.4$ [34, 35]. Interestingly, a novel wurtzite-type po-

lar magnetic metal, which hosts a metastable, zero-field Néel-type skyrmion lattice at RT, was discovered at $x = 0.5$ of Co-F5GT [36, 37]. The aforementioned observations of the Co-F5GT system highlight its immense tunability and capacity for unusual magnetic properties and could render applications in next-generation spintronics.

Despite the reports of exotic magnetic textures such as the chiral soliton lattices and skyrmions in F5GT or Co-F5GT [36, 38, 39], there is a scarcity of information from neutron scattering studies of these systems. The challenge of growing single crystals large enough for neutron experiments hinders the timely investigations of the magnetic properties of Co-F5GT. Here, we demonstrate the applicability of utilizing the element specific, resonant magnetic x-ray scattering (RMXS) technique [40–43] to investigate the bulk magnetic properties of a specific Co-F5GT single crystal at $x = 0.45(1)$. By tuning the x-ray energy $E = \hbar\omega$ to either the Fe L edges or Co L edges, our study determines the contribution from both the Fe and Co spin moments to the magnetic order. In addition, our scattering data affirms the A-type AFM order, with a Néel temperature $T_N \sim 340$ K and an out-of-plane moment direction. The influence of external magnetic fields on the AFM ground state is also explored and found to be consistent with magnetization measurements.

Single crystals of Co-F5GT at $x = 0.45(1)$ (labeled here as Co45-F5GT) were synthesized using the chemical vapor transfer technique [30, 31, 44]. The chemical composition of the samples was verified by energy dispersive x-ray spectroscopy, with the cation deficiency

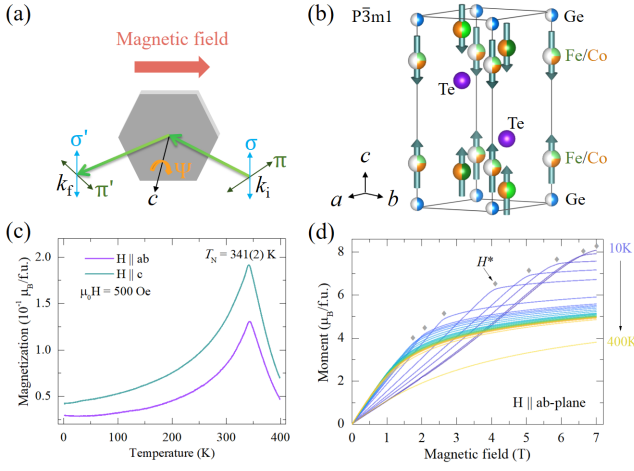


FIG. 1. (Color online) (a) The schematic of the resonant magnetic x-ray scattering (RMXS) experiment on a Co doped Fe_5GeTe_2 single crystal at $x = 0.45(1)$ ($(\text{Fe}_{0.55}\text{Co}_{0.45})_{5-\delta}\text{GeTe}_2$, Co45-F5GT). (b) The crystal structure of Co45-F5GT, with the AA stacking order [34, 36, 37]. (c) Temperature dependent magnetization of Co45-F5GT. (d) In-plane isothermal magnetization of Co45-F5GT at varying temperatures. The H^* is the saturation field, beyond which the spin moments are fully polarized along the field direction with a saturation magnetization M_{sat} .

$|\delta| \leq 0.1$. The RMXS experiments were performed at the UE46_PGM-1 beamline at Helmholtz-Zentrum Berlin (HZB) and the 29-ID IEX beamline at Advanced Photon Source (APS) at Argonne National Laboratory. A horizontal scattering geometry is utilized with the sample lattice c direction lying within the scattering plane (Fig. 1(a)). The Bragg peaks $\mathbf{Q} = (H \cdot \frac{2\pi}{a}, K \cdot \frac{2\pi}{b}, L \cdot \frac{2\pi}{c})$ are defined in reciprocal lattice units (*r.l.u.*) with lattice parameters $a = b \approx 4.02 \text{ \AA}$ and $c \approx 9.80 \text{ \AA}$. The data are collected near the Fe and Co L edges to enhance the magnetic scattering signal [45–47]. The incoming x-ray is either horizontally polarized (H -pol or π -pol) or vertically polarized (V -pol or σ -pol), but the scattered x-rays are not analyzed. Therefore, both outgoing σ' -pol and π' -pol channels will contribute to the scattered intensity, which can be written as [42, 43]:

$$I_{\mu\nu} \propto \left| \sum_j e^{i\mathbf{Q}\cdot\mathbf{r}_j} (\mathbf{e}_\mu \times \mathbf{e}_\nu^*) \cdot \mathbf{m}_j F(E) \right|^2, \quad (1)$$

to first order in the magnetic moment \mathbf{m}_j of the ion located at site \mathbf{r}_j within the unit cell. \mathbf{e}_μ ($\mu = \sigma$ or π) and \mathbf{e}_ν ($\nu = \sigma'$ or π') are unit vectors along the polarization of the electric field component of the incident and outgoing x-ray beams, respectively. $F(E)$ is the non-local, photon energy dependent scattering tensor. Since the polarization of the scattered light is not analyzed, the measured intensities are $I_H = I_\pi \equiv I_{\pi\sigma'} + I_{\pi\pi'}$ and $I_V = I_\sigma \equiv I_{\sigma\sigma'} + I_{\sigma\pi'}$.

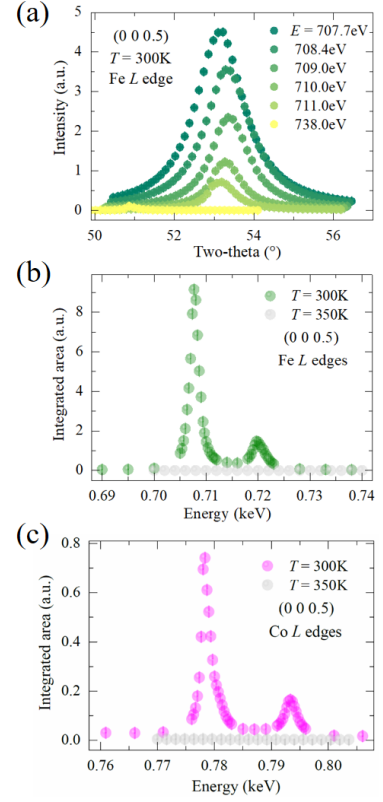


FIG. 2. (Color online) Photon energy dependence of the (0, 0, 0.5) peak at $T = 300 \text{ K}$ or 350 K . (a) The (0, 0, 0.5) peak at $T = 300 \text{ K}$ near the Fe L edges. Maximum intensity is observed at Fe L_{III} edge ($E = 707.7 \text{ eV}$). (b)-(c) Energy dependent integrated area of the (0, 0, 0.5) peak at both 300 K and 350 K , near the Fe L edges (b) and Co L edges (c), respectively.

The F5GT compound is composed of three identical layers with the rhombohedral layer stacking (space group $R\bar{3}m$), labelled as ABC-stacking [30]. It was experimentally established that the stacking order in F5GT is susceptible to external perturbations [34, 36, 48]. Upon replacing Fe with Co in F5GT, when $x \geq 0.4$, the crystal structure undergoes a transition from ABC-stacking to AA-stacking (space group $P\bar{3}m1$, as shown in Fig. 1(b)) [34]. Meanwhile, the magnetic ground state evolves from FM at $x < 0.4$ to AFM when $x \geq 0.4$. Our magnetization measurements on the Co45-F5GT sample confirm an AFM order, with $T_N = 341(2) \text{ K}$ (Fig. 1(c)). It is worth emphasizing that a unique type of stacking order, labelled as AA'-stacking, was reported recently at $x = 0.5$ [36, 37]. Néel-type skyrmions were identified at this doping, because of the AA'-stacking order which breaks the inversion symmetry and therefore features a bulk Dzyaloshinskii–Moriya interaction [49, 50]. The spin structures of Co-F5GT, however, have not yet been investigated by bulk scattering techniques. Particularly, the magnetic ground state, including the spin moment direction, shows a strong dependence on the Co doping

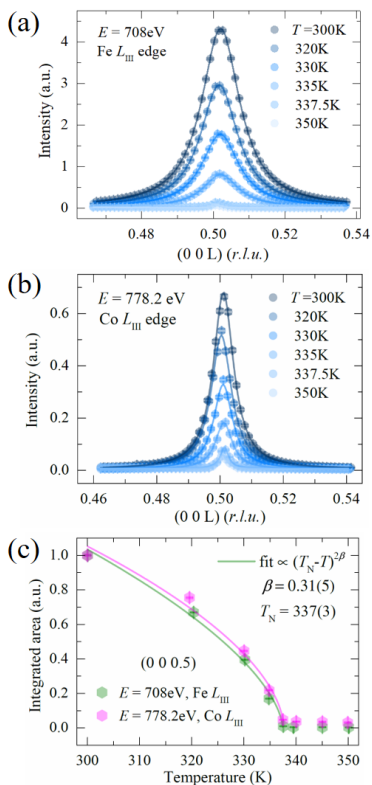


FIG. 3. (Color online) Temperature dependence of the (0, 0, 0.5) peak, at different energies: (a) Fe L_{III} edge, $E = 708$ eV, (b) Co L_{III} edge, $E = 778.2$ eV. Solid lines in (a)-(b) are Lorentzian fits to the peak intensity. (c) Power law fits to the integrated area of the (0, 0, 0.5) peak at both Fe and Co L_{III} edges. For better comparison, the data is normalized to 1 at $T = 300$ K.

level x [30, 31, 36, 38]. Consequently, it is important to investigate the magnetic properties of Co-F5GT by using a direct, bulk-sensitive, element-specific scattering technique such as RMXS.

Our RMXS experiments were performed on Co45-F5GT single crystals with the AA-stacking sequence (P3m1, Fig. 1(b)). A strong peak is identified at the structurally forbidden Bragg peak position $\mathbf{Q}_0 = (0, 0, 0.5)$ below the magnetic onset temperature. To understand fully the nature of this reflection, we present a thorough study of its dependence on x-ray energy, polarization, temperature and magnetic field. Fig. 2 shows the x-ray energy dependence of the \mathbf{Q}_0 reflection. Resonant peak profiles were recorded near both the Fe and Co L_{III} or L_{II} edges (Fe $L_{III} \sim 708$ eV, Fe $L_{II} \sim 720$ eV, Co $L_{III} \sim 778$ eV and Co $L_{II} \sim 793$ eV) [45–47]. A single energy dependent peak profile is evident near both the Fe and Co L_{III} (L_{II}) edges. This resonance in photon energy is a strong signature of the magnetic nature of the \mathbf{Q}_0 peak [42, 43, 45–47]. To support this argument further, the temperature dependence of the \mathbf{Q}_0 peak at the resonance energies (both Fe and Co L_{III} edges) was

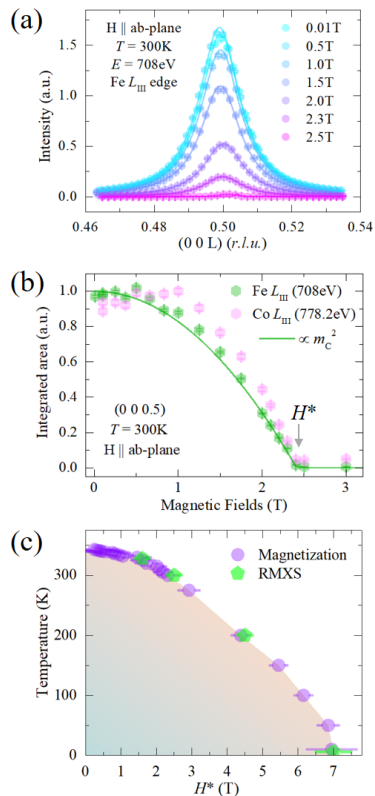


FIG. 4. (Color online) Magnetic field dependence of the (0, 0, 0.5) peak on resonance. (a) The (0, 0, 0.5) peak at $T = 300$ K and $E = 708$ eV, collected under select magnetic fields. Solid lines are Lorentzian fits to the peak intensity. (b) Field dependence of the integrated area of the (0, 0, 0.5) peak at 300 K, at both Fe and Co L_{III} edges. The peak intensity is completely suppressed beyond $H^* = 2.4(1)$ T. The green line is a fit to the data by assuming the intensity is proportional to the c component of the magnetization squared m_c^2 . For better comparison, the data is normalized to 1 at zero field. (c) Phase diagram of the temperature dependent H^* , from both the magnetization and RMXS measurements.

also examined, as shown in Figs. 2-3. With increasing temperature, the peak intensity at either the Fe or the Co L_{III} edge is becoming vanishingly small and independent of temperature above the transition temperature $T_N = 337(3)$ K (Fig. 3) [44].

Both the energy and temperature dependent studies in Figs. 2-3 demonstrate the magnetic nature of the (0, 0, 0.5) peak, which is in agreement with the AFM behavior from the magnetization in Fig. 1(c). This is further supported by studying the magnetic field dependence of the \mathbf{Q}_0 peak on resonance (at both Fe and Co L_{III} edges), examined at select temperatures (Fig. 4). The field was applied in the ab plane of the sample (Fig. 1(a)). With increasing magnetic field, the \mathbf{Q}_0 peak intensity is gradually suppressed and reaches almost zero when $H \geq H^*$. This can be easily understood since the applied magnetic fields are polarizing the spins along the

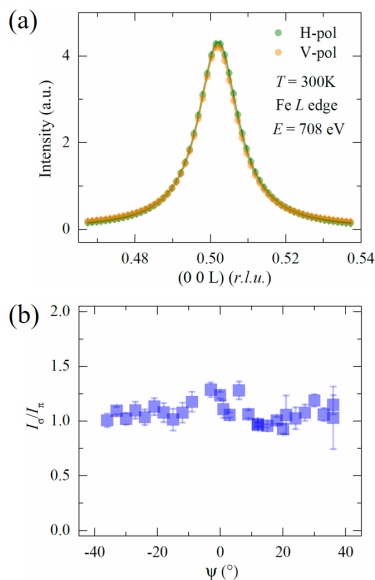


FIG. 5. (Color online) (a) The $(0, 0, 0.5)$ peak, collected at 708 eV and 300K, with the incoming x-ray either horizontally (π -pol) or vertically (σ -pol) polarized. $I_\sigma = I_\pi$ is observed. (b) The intensity ratio $I_\sigma/I_\pi \approx 1$ in a wide range of azimuthal angle Ψ , where $\Psi = 0$ is defined when the $[1\ 0\ 0]$ direction is parallel to the scattering plane.

field direction. When the magnetic moments are fully polarized under $H \geq H^*$, the magnetic structure enters into the polarized FM state and hence the peak intensity at \mathbf{Q}_0 disappears. By assuming that the measured peak intensity is proportional to the c component of the magnetic moment squared m_c^2 , which equals $M_{\text{sat}}^2 - M_{\text{ab}}^2$ from the magnetization data in Fig. 1(d), an excellent agreement is found between the field dependence of the resonant peak intensity at Fe L_{III} edge and the measured magnetization squared (green line in Fig. 4(b)). Specifically, the H^* values at different temperatures inferred from both the RMXS data and the magnetization data also match each other excellently, which are summarized and plotted as the phase diagram in Fig. 4(c).

Combining all evidence, our study confirms the AFM nature of Co45-F5GT with a propagation vector $\mathbf{Q}_0 = (0, 0, 0.5)$ and a transition temperature $T_N \sim 340$ K. The similar behavior of the magnetic peak at both the Fe or Co L edges indicates an important contribution from the Co spin moments in Co-F5GT. This explains why the saturation moment of Co45-F5GT at 10 K (Fig. 1(d))— $M_{\text{sat}} \sim 8 \mu_B$ per formula unit ($f.u.$)—is only slightly smaller than the value of $M_{\text{sat}} \sim 10 \mu_B$ per $f.u.$ in F5GT ($x = 0$). By assuming the average Fe magnetic moment is unchanged ($\sim 2 \mu_B/\text{Fe}$) [30, 31, 36, 48], the average Co spin moment contribution to the magnetization is estimated to be $\sim 1.1 \mu_B/\text{Co}$ in Co45-F5GT. Clearly, identifying the presence of an ordered magnetic moment at the Co site is an important result of our work.

Another important piece of information is the magnetic moment direction, specifically the magnetic structure below T_N . This can be inferred from the representational analysis [51], the photon polarization and azimuthal dependence of the RMXS data. The magnetic representation of the crystallographic sites of Fe or Co can be decomposed in terms of the irreducible representations (IRs) [51], with the propagation vector $\mathbf{Q}_0 = (0, 0, 0.5)$ (Table I): $\Gamma_{\text{Mag}} = 1\Gamma_2^1 + 1\Gamma_3^1 + 1\Gamma_5^2 + 1\Gamma_6^2$, where Γ_2, Γ_3 are one-dimensional IRs with moments pointing parallel to the c axis and Γ_5, Γ_6 are two-dimensional IRs with basis vectors lying in the ab -plane.

Considering the AFM nature, only the solutions from Γ_3 and Γ_5 are possible. Experimentally, the magnetic peak intensity at the \mathbf{Q}_0 position remains the same with either σ or π polarized incoming x-rays (Fig. 5(a)), which implies $I_\pi = I_\sigma$:

$$\left| \sum_j e^{i\mathbf{Q}\cdot\mathbf{r}_j} \mathbf{k}_f \cdot \mathbf{m}_j \right|^2 = \left| \sum_j e^{i\mathbf{Q}\cdot\mathbf{r}_j} \mathbf{k}_i \cdot \mathbf{m}_j \right|^2 + \left| \sum_j e^{i\mathbf{Q}\cdot\mathbf{r}_j} \mathbf{e}_\sigma \cdot \mathbf{m}_j \right|^2 \quad (2)$$

where \mathbf{k}_i and \mathbf{k}_f are the unit vectors along the incoming and reflected photon wave-vector directions, respectively. The azimuthal Ψ dependence of the \mathbf{Q}_0 peak was performed by rotating the sample about the \mathbf{Q}_0 direction, which is parallel to the c -axis (Fig. 1(a)), and measuring the peak intensity for both polarizations. Clearly, $I_\sigma \approx I_\pi$ is maintained over a broad range of the Ψ angle (Fig. 5(b)). This rules out the possible contribution from Γ_5 since the presence of in-plane moments will manifest as an angle-dependent azimuthal scan by virtue of rotating the projections shown in Equation (2). It is evident that only the solution from Γ_3 satisfies Equation (2) ($I_\pi = I_\sigma$), regardless of the Ψ angle, since the magnet moments pointing along the c direction are parallel to the rotation axis along the \mathbf{Q}_0 direction. From these arguments, the experimental data determine an A-type AFM order with Ising moments in Co45-F5GT, as depicted in Fig. 1(b).

Our RMXS study together with the magnetization data on the Co45-F5GT single crystals confirm the long-range AFM ground state. Under moderate magnetic fields ($H < H^*$), this AFM state is still maintained, since the $(0, 0, 0.5)$ magnetic peak is only gradually weakened in magnitude, but without becoming incommensurate or significantly broadened in peak width. This suggests that it is unlikely to have the magnetic field induced exotic spin textures in Co45-F5GT with the AA-stacking order, unlike the novel AA'-stacked structure hosting Néel-type skyrmion lattices in Co-F5GT at $x = 0.50$ [36, 37]. The contrasting magnetic textures in Co-F5GT, albeit with the similar Co doping level $x = 0.45$ or $x = 0.5$, highlight the essential role of the underlying lattice symmetry, as well as the contribution from the Co spin moments. Additionally, the Co magnetic moments appear to play

IR	BV Atom	BV components			
		$m_{\parallel a}$	$m_{\parallel b}$	$m_{\parallel c}$	
Γ_2	ψ_1	1	0	0	1
		2	0	0	1
Γ_3	ψ_2	1	0	0	1
		2	0	0	-1
Γ_5	ψ_3	1	0	-1	0
		2	0	1	0
	ψ_4	1	-2	-1	0
		2	2	1	0
Γ_6	ψ_5	1	2	1	0
		2	2	1	0
	ψ_6	1	0	-1	0
		2	0	-1	0

TABLE I. Basis vectors for the space group $P\bar{3}m1$ with the propagation vector $\mathbf{Q}_0 = (0, 0, 0.5)$. The decomposition of the magnetic representation for the Fe1/Co1 site is $\Gamma_{\text{Mag}} = 1\Gamma_2^1 + 1\Gamma_3^1 + 1\Gamma_5^2 + 1\Gamma_6^2$. The two different atoms of the Fe1/Co1 site within the unit cell are defined: atom1, (0, 0, 0.2318); atom2, (0, 0, 0.7682). The results from the irreducible representations analysis for the other Fe/Co sites are similar.

an essential role for the enhancement of the magnetic transition temperature in Co-F5GT, in contrast to the nonmagnetic dilution in Ni doped F5GT [48].

In summary, our RMXS study together with the magnetization measurements on the Co45-F5GT sample confirms the Ising nature of the A-type AFM spin structure, with a propagation vector $\mathbf{Q}_0 = (0, 0, 0.5)$ and a Néel temperature $T_N \sim 340$ K. The unique, element specific characteristics of RMXS, observed through tuning the photon energy, highlight the sizable contribution from the Co spin moments to the AFM order. In addition, the magnetic ground state under the in-plane magnetic fields has also been investigated, suggesting the critical role of the underlying lattice symmetry for stabilizing unusual spin textures. Our work highlights the applicability of the RMXS technique to study the magnetic properties in Co-F5GT and other quasi-2D vdW magnets.

X.C. wishes to thank Fanny M. Rodolakis for assistance before and during the RMXS experiment carried out at the Advanced Photon Source. Work at University of California, Berkeley and the Lawrence Berkeley National Laboratory was funded by the U.S. Department of Energy, Office of Science, Office of Basic Energy Sciences, Materials Sciences and Engineering Division under Contract No. DE-AC02-05-CH11231 within the Quantum Materials Program (KC2202). Work at UC San Diego was supported by the National Science Foundation under Grant No. DMR-2145080. This research used resources of the Advanced Photon Source, a U.S. Department of Energy (DOE) Office of Science User Facility at Argonne National Laboratory and is based on research supported by the U.S. DOE Office of Science-Basic Energy Sciences, under Contract No. DE-AC02-06CH11357. We thank

HZB for the allocation of synchrotron radiation beamtime. A.F. was supported by the Alfred P. Sloan Foundation (FG-2020-13773) and the Research Corporation for Science Advancement via the Cottrell Scholar Award (27551).

* xiangchen@berkeley.edu

† afrano@ucsd.edu

- [1] J.-G. Park, Opportunities and challenges of 2D magnetic van der Waals materials: magnetic graphene?, *Journal of Physics: Condensed Matter* **28**, 301001 (2016).
- [2] K. S. Novoselov, A. Mishchenko, A. Carvalho, and A. H. C. Neto, 2D materials and van der Waals heterostructures, *Science* **353**, aac9439 (2016).
- [3] Y. Liu, N. O. Weiss, X. Duan, H.-C. Cheng, Y. Huang, and X. Duan, Van der Waals heterostructures and devices, *Nature Reviews Materials* **1**, 16042 (2016).
- [4] K. S. Burch, D. Mandrus, and J.-G. Park, Magnetism in two-dimensional van der Waals materials, *Nature* **563**, 47 (2018).
- [5] M. Gibertini, M. Koperski, A. F. Morpurgo, and K. S. Novoselov, Magnetic 2D materials and heterostructures, *Nature Nanotechnology* **14**, 408 (2019).
- [6] C. Gong and X. Zhang, Two-dimensional magnetic crystals and emergent heterostructure devices, *Science* **363**, 10.1126/science.aav4450 (2019).
- [7] K. F. Mak, J. Shan, and D. C. Ralph, Van der Waals heterostructures for spintronics and opto-spintronics, *Nature Reviews Physics* **1**, 646 (2019).
- [8] L. Du, T. Hasan, A. Castellanos-Gomez, G.-B. Liu, Y. Yao, C. N. Lau, and Z. Sun, Engineering symmetry breaking in 2D layered materials, *Nature Reviews Physics* **3**, 193 (2021).
- [9] J. F. Sierra, J. Fabian, R. K. Kawakami, S. Roche, and S. O. Valenzuela, Van der Waals heterostructures for spintronics and opto-spintronics, *Nature Nanotechnology* **16**, 856 (2021).
- [10] Y. Cao, V. Fatemi, S. Fang, K. Watanabe, T. Taniguchi, E. Kaxiras, and P. Jarillo-Herrero, Unconventional superconductivity in magic-angle graphene superlattices, *Nature* **556**, 43 (2018).
- [11] Q. Ma, S.-Y. Xu, H. Shen, D. MacNeill, V. Fatemi, T.-R. Chang, A. M. Mier Valdivia, S. Wu, Z. Du, C.-H. Hsu, S. Fang, Q. D. Gibson, K. Watanabe, T. Taniguchi, R. J. Cava, E. Kaxiras, H.-Z. Lu, H. Lin, L. Fu, N. Gedik, and P. Jarillo-Herrero, Observation of the nonlinear Hall effect under time-reversal-symmetric conditions, *Nature* **565**, 337 (2019).
- [12] K. Kang, T. Li, E. Sohn, J. Shan, and K. F. Mak, Non-linear anomalous Hall effect in few-layer WTe₂, *Nature Materials* **18**, 324 (2019).
- [13] V. Carteaux, D. Brunet, G. Ouvrard, and G. Andre, Crystallographic, magnetic and electronic structures of a new layered ferromagnetic compound Cr₂Ge₂Te₆, *Journal of Physics: Condensed Matter* **7**, 69 (1995).
- [14] C. Gong, L. Li, Z. Li, H. Ji, A. Stern, Y. Xia, T. Cao, W. Bao, C. Wang, Y. Wang, Z. Q. Qiu, R. J. Cava, S. G. Louie, J. Xia, and X. Zhang, Discovery of intrinsic ferromagnetism in two-dimensional van der Waals crystals, *Nature* **546**, 265 (2017).

- [15] M. A. McGuire, H. Dixit, V. R. Cooper, and B. C. Sales, Coupling of Crystal Structure and Magnetism in the Layered, Ferromagnetic Insulator CrI_3 , *Chem. Mater.* **27**, 612 (2015).
- [16] B. Huang, G. Clark, E. Navarro-Moratalla, D. R. Klein, R. Cheng, K. L. Seyler, D. Zhong, E. Schmidgall, M. A. McGuire, D. H. Cobden, W. Yao, D. Xiao, P. Jarillo-Herrero, and X. Xu, Layer-dependent ferromagnetism in a van der Waals crystal down to the monolayer limit, *Nature* **546**, 270 (2017).
- [17] C.-Z. Chang, J. Zhang, X. Feng, J. Shen, Z. Zhang, M. Guo, K. Li, Y. Ou, P. Wei, L.-L. Wang, Z.-Q. Ji, Y. Feng, S. Ji, X. Chen, J. Jia, X. Dai, Z. Fang, S.-C. Zhang, K. He, Y. Wang, L. Lu, X.-C. Ma, and Q.-K. Xue, Experimental Observation of the Quantum Anomalous Hall Effect in a Magnetic Topological Insulator, *Science* **340**, 167 (2013).
- [18] Y. Deng, Y. Yu, M. Z. Shi, Z. Guo, Z. Xu, J. Wang, X. H. Chen, and Y. Zhang, Quantum anomalous Hall effect in intrinsic magnetic topological insulator MnBi_2Te_4 , *Science* **367**, 895 (2020).
- [19] B. Huang, M. A. McGuire, A. F. May, D. Xiao, P. Jarillo-Herrero, and X. Xu, Emergent phenomena and proximity effects in two-dimensional magnets and heterostructures, *Nature Materials* **19**, 1276 (2020).
- [20] Y. Guo, S. Zhou, and J. Zhao, Two-dimensional intrinsic ferromagnets with high Curie temperatures: synthesis, physical properties and device applications, *J. Mater. Chem. C* **9**, 6103 (2021).
- [21] H.-J. Deiseroth, K. Aleksandrov, C. Reiner, L. Kienle, and R. K. Kremer, Fe_3GeTe_2 and Ni_3GeTe_2 – Two New Layered Transition-Metal Compounds: Crystal Structures, HRTEM Investigations, and Magnetic and Electrical Properties, *European Journal of Inorganic Chemistry* **2006**, 1561 (2006).
- [22] B. Chen, J. Yang, H. Wang, M. Imai, H. Ohta, C. Michioka, K. Yoshimura, and M. Fang, Magnetic Properties of Layered Itinerant Electron Ferromagnet Fe_3GeTe_2 , *Journal of the Physical Society of Japan* **82**, 124711 (2013).
- [23] A. F. May, S. Calder, C. Cantoni, H. Cao, and M. A. McGuire, Magnetic structure and phase stability of the van der Waals bonded ferromagnet $\text{Fe}_{3-x}\text{GeTe}_2$, *Phys. Rev. B* **93**, 014411 (2016).
- [24] D. C. Freitas, R. Weht, A. Sulpice, G. Remenyi, P. Strobel, F. Gay, J. Marcus, and M. Núñez-Regueiro, Ferromagnetism in layered metastable $1T\text{-CrTe}_2$, *Journal of Physics: Condensed Matter* **27**, 176002 (2015).
- [25] X. Sun, W. Li, X. Wang, Q. Sui, T. Zhang, Z. Wang, L. Liu, D. Li, S. Feng, S. Zhong, H. Wang, V. Bouchiat, M. Nunez Regueiro, N. Rougemaille, J. Coraux, A. Purbawati, A. Hadj-Azzem, Z. Wang, B. Dong, X. Wu, T. Yang, G. Yu, B. Wang, Z. Han, X. Han, and Z. Zhang, Room temperature ferromagnetism in ultra-thin van der Waals crystals of $1T\text{-CrTe}_2$, *Nano Research* **13**, 3358 (2020).
- [26] Y. Deng, Y. Yu, Y. Song, J. Zhang, N. Z. Wang, Z. Sun, Y. Yi, Y. Z. Wu, S. Wu, J. Zhu, J. Wang, X. H. Chen, and Y. Zhang, Gate-tunable room-temperature ferromagnetism in two-dimensional Fe_3GeTe_2 , *Nature* **563**, 94 (2018).
- [27] Q. Li, M. Yang, C. Gong, R. V. Chopdekar, A. T. N'Diaye, J. Turner, G. Chen, A. Scholl, P. Shafer, E. Arenholz, A. K. Schmid, S. Wang, K. Liu, N. Gao, A. S. Admasu, S.-W. Cheong, C. Hwang, J. Li, F. Wang, X. Zhang, and Z. Qiu, Patterning-Induced Ferromagnetism of Fe_3GeTe_2 van der Waals Materials beyond Room Temperature, *Nano Letters* **18**, 5974 (2018).
- [28] J. Seo, D. Y. Kim, E. S. An, K. Kim, G.-Y. Kim, S.-Y. Hwang, D. W. Kim, B. G. Jang, H. Kim, G. Eom, S. Y. Seo, R. Stania, M. Muntwiler, J. Lee, K. Watanabe, T. Taniguchi, Y. J. Jo, J. Lee, B. I. Min, M. H. Jo, H. W. Yeom, S.-Y. Choi, J. H. Shim, and J. S. Kim, Nearly room temperature ferromagnetism in a magnetic metal-rich van der Waals metal, *Science Advances* **6**, 10.1126/sciadv.aay8912 (2020).
- [29] J. Stahl, E. Shlaen, and D. Johrendt, The van der Waals Ferromagnets $\text{Fe}_{5-\delta}\text{GeTe}_2$ and $\text{Fe}_{5-\delta-x}\text{Ni}_x\text{GeTe}_2$ – Crystal Structure, Stacking Faults, and Magnetic Properties, *Zeitschrift für anorganische und allgemeine Chemie* **644**, 1923 (2018).
- [30] A. F. May, D. Ovchinnikov, Q. Zheng, R. Hermann, S. Calder, B. Huang, Z. Fei, Y. Liu, X. Xu, and M. A. McGuire, Ferromagnetism Near Room Temperature in the Cleavable van der Waals Crystal Fe_5GeTe_2 , *ACS Nano* **13**, 4436 (2019).
- [31] H. Zhang, R. Chen, K. Zhai, X. Chen, L. Caretta, X. Huang, R. V. Chopdekar, J. Cao, J. Sun, J. Yao, R. Birgeneau, and R. Ramesh, Itinerant ferromagnetism in van der Waals $\text{Fe}_{5-x}\text{GeTe}_2$ crystals above room temperature, *Phys. Rev. B* **102**, 064417 (2020).
- [32] K. Yamagami, Y. Fujisawa, B. Driesen, C. H. Hsu, K. Kawaguchi, H. Tanaka, T. Kondo, Y. Zhang, H. Wadati, K. Araki, T. Takeda, Y. Takeda, T. Muro, F. C. Chuang, Y. Niimi, K. Kuroda, M. Kobayashi, and Y. Okada, Itinerant ferromagnetism mediated by giant spin polarization of the metallic ligand band in the van der Waals magnet Fe_5GeTe_2 , *Phys. Rev. B* **103**, L060403 (2021).
- [33] X. Wu, L. Lei, Q. Yin, N.-N. Zhao, M. Li, Z. Wang, Q. Liu, W. Song, H. Ma, P. Ding, Z. Cheng, K. Liu, H. Lei, and S. Wang, Direct observation of competition between charge order and itinerant ferromagnetism in the van der Waals crystal $\text{Fe}_{5-x}\text{GeTe}_2$, *Phys. Rev. B* **104**, 165101 (2021).
- [34] A. F. May, M.-H. Du, V. R. Cooper, and M. A. McGuire, Tuning magnetic order in the van der Waals metal Fe_5GeTe_2 by cobalt substitution, *Phys. Rev. Materials* **4**, 074008 (2020).
- [35] C. Tian, F. Pan, S. Xu, K. Ai, T. Xia, and P. Cheng, Tunable magnetic properties in van der Waals crystals $(\text{Fe}_{1-x}\text{Co}_x)_5\text{GeTe}_2$, *Applied Physics Letters* **116**, 202402 (2020).
- [36] H. Zhang, Y.-T. Shao, R. Chen, X. Chen, S. Susarla, D. Raftrey, J. T. Reichanadter, L. Caretta, X. Huang, N. S. Settineri, Z. Chen, J. Zhou, E. Bourret-Courchesne, P. Ercius, J. Yao, P. Fischer, J. B. Neaton, D. A. Muller, R. J. Birgeneau, and R. Ramesh, A room temperature polar magnetic metal, *Phys. Rev. Materials* **6**, 044403 (2022).
- [37] H. Zhang, D. Raftrey, Y.-T. Chan, Y.-T. Shao, R. Chen, X. Chen, X. Huang, J. T. Reichanadter, K. Dong, S. Susarla, L. Caretta, Z. Chen, J. Yao, P. Fischer, J. B. Neaton, W. Wu, D. A. Muller, R. J. Birgeneau, and R. Ramesh, Room-temperature skyrmion lattice in a layered magnet $(\text{Fe}_{0.5}\text{Co}_{0.5})_5\text{GeTe}_2$, *Science Advances* **8**, eabm7103 (2022).
- [38] T. T. Ly, J. Park, K. Kim, H.-B. Ahn, N. J. Lee, K. Kim,

- T.-E. Park, G. Duvjir, N. H. Lam, K. Jang, C.-Y. You, Y. Jo, S. K. Kim, C. Lee, S. Kim, and J. Kim, Direct Observation of Fe-Ge Ordering in $\text{Fe}_{5-x}\text{GeTe}_2$ Crystals and Resultant Helimagnetism, *Advanced Functional Materials* **31**, 2009758 (2021).
- [39] Y. Gao, Q. Yin, Q. Wang, Z. Li, J. Cai, T. Zhao, H. Lei, S. Wang, Y. Zhang, and B. Shen, Spontaneous (Anti)meron Chains in the Domain Walls of van der Waals Ferromagnetic $\text{Fe}_{5-x}\text{GeTe}_2$, *Advanced Materials* **32**, 2005228 (2020).
- [40] M. Blume, Magnetic scattering of x rays (invited), *Journal of Applied Physics* **57**, 3615 (1985).
- [41] J. P. Hannon, G. T. Trammell, M. Blume, and D. Gibbs, X-Ray Resonance Exchange Scattering, *Phys. Rev. Lett.* **61**, 1245 (1988).
- [42] J. Fink, E. Schierle, E. Weschke, and J. Geck, Resonant elastic soft x-ray scattering, *Reports on Progress in Physics* **76**, 056502 (2013).
- [43] R. Comin and A. Damascelli, Resonant X-Ray Scattering Studies of Charge Order in Cuprates, *Annual Review of Condensed Matter Physics* **7**, 369 (2016).
- [44] The ~ 4 K smaller T_N , when comparing the number from the scattering data to the magnetization study, is likely due to the errors from the different thermal couples and/or the beam damage to the samples.
- [45] C. Kao, J. B. Hastings, E. D. Johnson, D. P. Siddons, G. C. Smith, and G. A. Prinz, Magnetic-resonance exchange scattering at the iron L_{II} and L_{III} edges, *Phys. Rev. Lett.* **65**, 373 (1990).
- [46] Y. Yamasaki, D. Morikawa, T. Honda, H. Nakao, Y. Murakami, N. Kanazawa, M. Kawasaki, T. Arima, and Y. Tokura, Dynamical process of skyrmion-helical magnetic transformation of the chiral-lattice magnet FeGe probed by small-angle resonant soft x-ray scattering, *Phys. Rev. B* **92**, 220421 (2015).
- [47] Y. W. Windsor, C. Piamonteze, M. Ramakrishnan, A. Scaramucci, L. Rettig, J. A. Huever, E. M. Bothschafter, N. S. Bingham, A. Alberca, S. R. V. Avula, B. Noheda, and U. Staub, Magnetic properties of strained multiferroic CoCr_2O_4 : A soft x-ray study, *Phys. Rev. B* **95**, 224413 (2017).
- [48] X. Chen, Y.-T. Shao, R. Chen, S. Susarla, T. Hogan, Y. He, H. Zhang, S. Wang, J. Yao, P. Ercius, D. A. Muller, R. Ramesh, and R. J. Birgeneau, Pervasive beyond Room-Temperature Ferromagnetism in a Doped van der Waals Magnet, *Phys. Rev. Lett.* **128**, 217203 (2022).
- [49] I. Dzyaloshinsky, A thermodynamic theory of “weak” ferromagnetism of antiferromagnetics, *Journal of Physics and Chemistry of Solids* **4**, 241 (1958).
- [50] T. Moriya, Anisotropic Superexchange Interaction and Weak Ferromagnetism, *Phys. Rev.* **120**, 91 (1960).
- [51] A. Wills, A new protocol for the determination of magnetic structures using simulated annealing and representational analysis (SARAh), *Physica B: Condensed Matter* **276-278**, 680 (2000).